



A human inspired handover policy using Gaussian Mixture Models and haptic cues

Antonis Sidiropoulos^{1,2} · Efi Psomopoulou^{1,2} · Zoe Doulgeri^{1,2} 

Received: 30 December 2016 / Accepted: 29 January 2018
© Springer Science+Business Media, LLC, part of Springer Nature 2018

Abstract

A handover strategy is proposed that aims at natural and fluent robot to human object handovers. For the approaching phase, a globally asymptotically stable dynamical system (DS) is utilized, trained from human demonstrations and exploiting the existence of mirroring in the human wrist motion. The DS operates in the robot task space thus achieving independence with respect to the robot platform, encapsulating the position and orientation of the human wrist within a single DS. It is proven that the motion generated by such a DS, having as target the current wrist pose of the receiver's hand, is bounded and converges to the previously unknown handover location. Haptic cues based on load estimates at the robot giver ensure full object load transfer before grip release. The proposed strategy is validated with simulations and experiments in real settings.

Keywords Programming by Demonstration · Gaussian Mixture Model · Physical human-robot interaction · Haptic communication

1 Introduction

The recent technological advancements in robotics are harbinger of the great influence that robots will have on human activities in the near future. Nowadays, the idea of having robots as assistants in domestic environments, particularly to aid people with handicaps and cognitive impair-

This is one of the several papers published in *Autonomous Robots* comprising the Special Issue on Learning for Human-Robot Collaboration.

The research leading to these results has received funding from the European Community's Framework Programme Horizon 2020 under Grant Agreement No 643433 RAMCIP.

Electronic supplementary material The online version of this article (<https://doi.org/10.1007/s10514-018-9705-x>) contains supplementary material, which is available to authorized users.

✉ Zoe Doulgeri
doulgeri@iti.gr; doulgeri@eng.auth.gr

Antonis Sidiropoulos
antosidi@iti.gr; antosidi@auth.gr

Efi Psomopoulou
efipsom@iti.gr; efipsom@eng.auth.gr

¹ Center for Research and Technology Hellas (CERTH),
57001 Thessaloniki, Greece

² Department of Electrical and Computer Engineering, Aristotle
University of Thessaloniki, 54124 Thessaloniki, Greece

ments, becomes increasingly popular. In this context of human-robot interaction, handovers occur quite frequently, therefore the necessity arises for seamless, reliable and natural handover control strategies (Bischoff and Guhl 2010).

The handover process is comprised of two main phases, the approaching phase, where both the giver and receiver extend their hands to reach each other, and the haptic interaction phase, where the joint grasp and the object load transfer take place. The approaching phase aims at moving the robotic arm in a natural and seamless way that is in accordance with human preferences (Waldhart et al. 2015; Prada et al. 2013; Huber et al. 2008; Cakmak et al. 2011; Strabala et al. 2013). Studies on the object load transfer analyze the haptic interaction which involves the relationship between the grip forces applied on the object and the load force as well as the temporal coordination between the participants (Mason and MacKenzie 2005; Chan et al. 2012, 2013; Kim et al. 2002).

For the approaching phase, dynamical systems have been proposed as an effective means to encode the human wrist motion. Two of the most prevalent approaches making use of dynamical systems for learning non-linear dynamics of discrete motions, like human motion, are the Dynamical Systems with Gaussian Mixture Models (DS with GMM) (Gribovskaya et al. 2011; Khansari-Zadeh and Billard 2010; Hersch et al. 2008) and the Dynamic Movement Primitives (DMP) (Ijspeert et al. 2002; Prada et al. 2014; Prada and

Remazeilles 2012; Prada et al. 2013; Pastor et al. 2009). As opposed to DS with GMM, DMPs may be trained even from one sample trajectory, i.e., the dynamical system learns essentially a specific trajectory and then uses a phase variable, which operates as an implicit clock, to shape its motion between a start and end pose according to the learned trajectory. Consequently DMPs exhibit a stereotypical behavior from all start points. However, DMP's trajectory-based representation can adapt to a newly demonstrated trajectory (Wang et al. 2016) even allowing optimization during execution with novel reinforcement learning algorithms (Pastor et al. 2012). Reinforcement learning has also been proposed in Kupcsik et al. (2015) combining absolute and preference feedback in a Bayesian framework to learn the reward function. On the other hand, DS with GMM follow a state space based learning of nonlinear dynamic systems and are not based on a phase variable like DMPs. As an advantage, a state space based representation can learn much more complex attractor landscapes; starting from different start points quite different behaviors can be created towards the same goal state (Pastor et al. 2012). As a disadvantage of DS with GMM, much more data is needed for learning, particularly in high dimensions (Pastor et al. 2012). In contrast to previous DS based approaches, we reduce the amount of data needed for training, by showing and exploiting the existence of mirroring in human motion via appropriate mirroring actions during execution. Thus, the amount of demonstrations required is reduced by 50% as they are confined to half of the space.

Dynamical Systems with Gaussian Mixture Models (GMM) have been successfully applied in robotics (Khansari-Zadeh and Billard 2010; Hersch et al. 2008; Gribovskaya et al. 2011; Kupcsik et al. 2010; Gribovskaya and Billard 2009; Shukla and Billard 2012). The DS proposed in Khansari-Zadeh and Billard (2010) is used for learning arbitrary discrete motions from a set of demonstrations, while ensuring global asymptotic stability at the target. However, the DS is applied by modeling only the Cartesian position of the robot end-effector or the robot joints, thus for different robotic platforms the correspondence problem has to be addressed. In Gribovskaya and Billard (2009) the position and orientation of the human wrist are encoded in two disjoint DS that fail to capture the correlation between them. A work that probabilistically encodes a pose in DS is Lang et al. (2015); however, the existing correlations between the task-space DOFs are lost in the mapping owing to the construction of the Gaussian Processes employed. Moreover, system stability is not examined. DMPs have also been used in Pastor et al. (2009) and (Pastor et al. 2011) for learning and generating desired end-effector poses as well as in Silverio et al. (2015) for the bimanual case utilizing the formulation of Ude et al. (2014). However, the defined DMPs are associated implicitly only through the common canonical system. As opposed to previous works with DS, we propose a sin-

gle DS for encoding pose dynamics, which also satisfies the necessary conditions to ensure global asymptotic stability at the target.

Another important aspect during the approaching phase is that, in general, both the giver and the receiver move. Hence, there is a time interval where their motions overlap temporarily. So far, this was not handled explicitly in the training process of a dynamical system. In fact, training of the DS is performed by feeding the DS with the giver's trajectory data with respect to the final exchange site that is revealed after the completion of the task. As, during execution, the final exchange site is unknown, the current pose of the receiver's hand is often given as the target of the DS, giving rise to deviations from the human trajectories, exhibiting even small oscillations in some cases (Prada and Remazeilles 2012; Widmann 2016). Consequently, methods are pursued to either find an estimate of the exchange site (Sisbot et al. 2010; Medina et al. 2016; Widmann 2016; Ben Amor et al. 2014), or mitigate this oscillation effects by introducing a velocity feedback term in the dynamical system (Prada and Remazeilles 2012). In Medina et al. (2016), the final exchange site is estimated by a linear dynamical system using least squares approximation and in Widmann (2016) a DMP is used to model the receiver's motion and predict the handover location. In Ben Amor et al. (2014) a single DMP is utilized to encode motions of both the giver and the receiver in joint space and a probabilistic distribution of the DMP parameters is used to allow predictions of the task space goal by observing partial trajectories of the human partner. However, the uncertainty associated with this prediction significantly shrinks after observing 60% of the movement. In contrast to previous works we propose training the DS with stationary targets; i.e. the receiver's hand is fixed in human demonstrations and only the giver moves towards him from a range of relative initial poses. This training method generalizes well for moving targets and hence does not require predictions of the final exchange site.

Another key feature of handover is the energy exchanged during the object load transfer. Human studies have shown that during the object transfer, the grip and load forces decreased for the giver and increased for the receiver while the duration of the load transfer stays below 500 ms (Mason and MacKenzie 2005; Kim et al. 2002; Huber et al. 2008). Therefore, appropriate timing and synchronization between the giver and receiver is required for safe object transfer. Controllers that take into account the recommendations from these studies have been proposed for a human-like haptic interaction (Chan et al. 2013; Pso-mopoulou and Doulgeri 2014). A human-inspired object load transfer strategy targeted at robot assistance to elderly is introduced in Pso-mopoulou and Doulgeri (2015). In this strategy, the giver is a stably grasping robotic hand under a control law that achieves dynamically a stable grasp equilibrium state via

fingertip rolling as well as accurate estimates of the object's weight (Arimoto 2008). It is shown that the object remains stable when jointly grasped by both hands and that the giver follows closely the receiver's lead via on-line estimates of the object's load. Thus, the giver opens its grip only when the object is safely transferred to the receiver. To the best of our knowledge, there are few works in the literature that tackle the entire handover process, that is both the approaching and object load transfer phase. In Shukla and Billard (2012) a coupled DS with GMM based controller is introduced, where two dynamical systems driving the hand and finger motions are coupled. In this work, the proposed DS is integrated with an object load transfer that adopts the basic concept introduced in Psomopoulou and Doulgeri (2015) and hence it is designed to succeed even in the case of unreliable receivers.

In summary, the main novelties introduced by our approach with respect to the state-of-the-art are:

- the proposed globally asymptotically stable DS with GMM that encodes the human wrist position and orientation in a single DS,
- the existence of mirroring with respect to the target plane is showed and exploited thus significantly reducing the amount of data needed for training,
- demonstrations are performed by fixing the receiver's hand as these data are shown to generalize well for a moving receiver's hand (target); hence there is no need to predict the final handover site and
- the integration of the DS motion generation with an object load transfer strategy ensures that the receiver has stably grasped the object before releasing it.

The approach is validated by both simulations and experiments in various cases.

The rest of the paper is organized as follows. Section 2 introduces the proposed stable DS encoding the human wrist motion and provides proofs of its global asymptotic stability in cases of a fixed as well as a moving target generated by another DS. Section 3 analyzes the mirroring existing in human wrist motions with respect to the target plane and the way it may be exploited during execution. Sections 4 and 5 describe the DS training and evaluation and the object load transfer strategy respectively. Sections 6 and 7 provide simulation and experimental results that demonstrate and evaluate the proposed approach in various cases. Unit quaternion preliminaries can be found in the Appendix.

2 The proposed stable DS encoding human wrist motion

2.1 Mathematical formulation

A Dynamical System with Gaussian Mixture Models is proposed to encode the human wrist motion during object

handovers by associating the position and orientation error of the wrist with respect to the target with the translational and angular velocity of the wrist:

$$V = f(\xi) \quad (1)$$

where

$$V = \begin{bmatrix} v^T & \omega^T \end{bmatrix} \quad (2)$$

with $v \in \mathfrak{R}^3$ being the translational velocity and $\omega \in \mathfrak{R}^3$ the angular velocity, and ξ is a state variable given by:

$$\xi = \begin{bmatrix} \tilde{p} & e_o^T \end{bmatrix} \quad (3)$$

where $\tilde{p} = (p - p_d)$ is the position error, $p, p_d \in \mathfrak{R}^3$ is the current and desired position and $e_o = \Delta\epsilon$ is the orientation error defined via (31) given the current and desired orientation $R, R_d \in SO(3)$ respectively. Preliminary knowledge on quaternions is summarized in the "Appendix".

Remark 1 Notice that Euler angles or the angle-axis parameterization could have been considered as alternatives for orientation representation as done in Khansari Zadeh and Billard (2009); Gribovskaya and Billard (2009) respectively. Nonetheless, these parameterizations introduce additional singularities and mapping multiplicities generating abrupt motions, thus affecting the training and accuracy of the final model, especially in case of large rotations. A possible recourse would be the use of unit quaternions. Still, unit quaternions have to satisfy constraints (23) and (24), which are usually imposed on the output of the dynamical system at a post-processing step (Pastor et al. 2009). To avoid such modifications on the output of the DS one could leverage the potential of GMM to associate different inputs with different outputs, provided there is an implicit relation between them, and impose these constraints by construction. In our case, we set the input of the DS as the position and orientation error, expressed via quaternions, which are calculated by the forward kinematics, consequently (23) holds. For the output we choose the linear and rotational velocity of the wrist which is related to the quaternion derivative via (29) and thus guarantees the satisfaction of constraint (24).

The dynamical system consists of K Gaussian functions whose parameters are learned using the set of demonstrations $\{\xi^{t,n}, V^{t,n}\}_{t=0, n=1}^{T_n, N}$, in order to find \hat{f} , the approximation of f in \mathfrak{R}^6 . We also require that \hat{f} is a stable estimate of f in \mathfrak{R}^6 , which means that: (1) it has a single attractor $\xi^* : \hat{f}(\xi^*) = 0$ and (2) any trajectory $\{\xi^t, V^t\}_{t=0}^T$ generated by \hat{f} converges asymptotically to $\xi^* : \lim_{t \rightarrow \infty} \xi(t) = \xi^* = 0, \forall \xi \in \mathfrak{R}^6$.

For each Gaussian function we define the parameters $\theta^k = \{\pi^k, \mu^k, \Sigma^k\}$, where π^k is the prior and

$$\mu^k = \begin{pmatrix} \mu_{\xi}^k \\ \mu_V^k \end{pmatrix} \text{ and } \Sigma^k = \begin{pmatrix} \Sigma_{\xi}^k & \Sigma_{\xi V}^k \\ \Sigma_{V\xi}^k & \Sigma_V^k \end{pmatrix}$$

are the mean and covariance matrix of the k_{th} Gaussian function. Collecting these parameters in $\theta = \{\theta^1 \dots \theta^K\}$, the dynamical system is given by:

$$V = \hat{f}(\xi; \theta) = \sum_{k=1}^K h^k(\xi) (A^k \xi + b^k) \quad (4)$$

where $A^k = \Sigma_{V\xi}^k (\Sigma_{\xi}^k)^{-1}$, $b^k = \mu_V^k - A^k \mu_{\xi}^k$, $h^k(\xi) = \frac{\pi^k P(\xi; \mu_{\xi}^k, \Sigma_{\xi}^k)}{\sum_{i=1}^K \pi^i P(\xi; \mu_{\xi}^i, \Sigma_{\xi}^i)}$ and $P(\xi; \mu_{\xi}^i, \Sigma_{\xi}^i)$ is given by the Gaussian probability function. Notice that the nonlinear weighting term $h^k(\xi)$ gives a measure of the relative influence of each Gaussian locally and takes values in the range (0, 1].

Theorem 1 Assuming a fixed target, p_d , Q_d , the dynamical system (4), with input ξ and output V given by (3) and (2) respectively, is globally asymptotically stable if $\forall k = 1 \dots K$ the following two conditions are satisfied:

$$b_i^k = -A_i^k \xi^* = 0 \quad (5)$$

$$A_i^k + (A_i^k)^T < 0 \quad (6)$$

Proof We propose the following candidate Lyapunov function W :

$$W = \frac{1}{2} \tilde{p}^T \tilde{p} + (Q - Q_d)^T (Q - Q_d) \quad (7)$$

W is positive definite with respect to p and Q which implies positive definiteness with respect to e_o . In fact, the potential term $(Q - Q_d)^T (Q - Q_d)$ can be written as $(Q - Q_d)^T (Q Q^T) (Q - Q_d) + e_o^T e_o$ where $Q Q^T$ is positive semi-definite since it is a projection matrix. The proof employs (33) and the equation $I_4 = J_Q J_Q^T + Q Q^T$ where I_4 is the identity matrix of dimension 4. The latter can be proved by direct mathematical manipulation utilizing (23) and the fact that $\hat{\epsilon} \hat{\epsilon} = \epsilon \epsilon^T - \epsilon^2 I_3$ where $\hat{\epsilon}$ denotes the skew symmetric matrix of vector ϵ (Murray and Sastry 1994).

Taking the time derivative along the solutions of (4) and utilizing (29) yields:

$$\dot{W} = (p - p_d)^T \dot{p} + (Q - Q_d)^T J_Q \omega.$$

Taking into account (33), \dot{W} becomes

$$\dot{W} = [\tilde{p}^T e_o^T] \begin{bmatrix} v \\ \omega \end{bmatrix}$$

which can be written as

$$\dot{W} = \xi^T \hat{f}(\xi).$$

Substituting $\hat{f}(\xi)$ from (4) and taking into account that $h^k(\xi) \in (0, 1] \forall k = 1 \dots K$ as well as (5), (6):

$$\dot{W} = \sum_{k=1}^K h^k(\xi) \xi^T \left(\frac{A^k + (A^k)^T}{2} \right) \xi < 0$$

The negative definiteness of \dot{W} implies the global asymptotic stability of the system (4). \square

Theorem 2 Two dynamical systems $V_1 = \hat{f}(\xi_1)$ and $V_2 = \hat{f}(\xi_2)$ given by (4), (3) and (2), with moving targets $p_{d1} = p_2$, $Q_{d1} = Q_2$ and $p_{d2} = p_1$, $Q_{d2} = Q_1$ respectively, are globally asymptotically stable in the origin, i.e. $\xi_1 = -\xi_2 = 0$, if $\forall k = 1 \dots K$ and for $i = 1, 2$ the following conditions are satisfied:

$$b_i^k = -A_i^k \xi^* = 0 \quad (8)$$

$$A_i^k + (A_i^k)^T < 0 \quad (9)$$

Theorem 2 states that the motion created by each DS, having as target the current pose of the other, will be bounded and converge to the same, previously unknown location, where the object handover will take place.

Proof We propose the following candidate Lyapunov function W :

$$W = \frac{1}{4} \tilde{p}_1^T \tilde{p}_1 + \frac{1}{2} (Q_1 - Q_2)^T (Q_1 - Q_2) + \frac{1}{4} \tilde{p}_2^T \tilde{p}_2 + \frac{1}{2} (Q_2 - Q_1)^T (Q_2 - Q_1) \quad (10)$$

W is positive definite with respect to p_1 , Q_1 and p_2 , Q_2 and by similar argument as in the proof of Theorem 1 we can show positive definiteness with respect to e_{o1} and e_{o2} .

Taking the time derivative of (10) we get:

$$\dot{W} = \tilde{p}_1^T \dot{p}_1 + \tilde{p}_2^T \dot{p}_2 + 2(Q_1 - Q_2)^T \dot{Q}_1 + 2(Q_2 - Q_1)^T \dot{Q}_2$$

Utilizing (29) yields:

$$\dot{W} = \tilde{p}_1^T \dot{p}_1 + (Q_1 - Q_2)^T J_{Q_1} \omega_1 + \tilde{p}_2^T \dot{p}_2 + (Q_2 - Q_1)^T J_{Q_2} \omega_2$$

Taking into account (33), \dot{W} becomes

$$\dot{W} = [\tilde{p}_1^T e_{o1}^T] \begin{bmatrix} v_1 \\ \omega_1 \end{bmatrix} + [\tilde{p}_2^T e_{o2}^T] \begin{bmatrix} v_2 \\ \omega_2 \end{bmatrix}$$

which can be written as

$$\dot{W} = \xi_1^T \hat{f}_1(\xi_1) + \xi_2^T \hat{f}_2(\xi_2)$$

resulting in:

$$\dot{W} = \sum_{i=1}^2 \sum_{k=1}^K h^k(\xi_i) \xi_i^T \left(\frac{A_i^k + (A_i^k)^T}{2} \right) \xi_i < 0$$

The negative definiteness of \dot{W} implies that the motion generated by the two DS will be globally stable and will eventually converge to the same pose. \square

2.2 Learning algorithm

To train the DS we use the Stable Estimator of Dynamical Systems (SEDS) learning method, presented in Khansari-Zadeh and Billard (2010), which can be directly extended to our proposed DS. Concretely, we learn the DS parameters by optimizing the following objective function:

$$\min_{\theta} J(\theta) = \frac{1}{2T} \sum_{n=1}^N \sum_{t=0}^{T_n} \|\hat{v}^{t,n} - v^{t,n}\|^2 \tag{11}$$

subject to the constraints $b^k = -A^k \xi^*$, $A^k + (A^k)^T < 0$, $\Sigma_{\xi}^k > 0$, $0 < \pi^k \leq 1$ and $\sum_{k=1}^K \pi^k, \forall k \in 1 \dots K$ where $T = \sum_{n=1}^N T_n$ is the total number of training points. The first two constraints are imposed to ensure the global stability of the model, while the last three stem from the nature of Gaussian Mixture Model. The optimization was performed using MATLAB’s “fmincon” function.

3 Mirroring in human wrist motion during handovers

Learning human like reaching motions, encoding both position and orientation, requires collecting data in 6D space. As the amount of data and demonstrations increase, so does the computational cost during training and execution. In this section, the hypothesis of mirroring in human handovers about an appropriately defined plane related to the target is made and validated, i.e., reflections of demonstrated trajectories recorded on half the space do not differ significantly from demonstrations recorded on the other side of the plane. As a consequence, demonstrations can be confined only in half space, hence the amount of data needed for training is halved speeding up the process of data collection and optimization. Moreover, half the number of Gaussians are needed to cover the trained space yielding a DS with reduced complexity, i.e.,

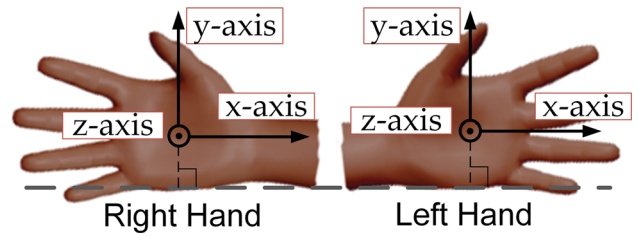


Fig. 1 Hand frame convention

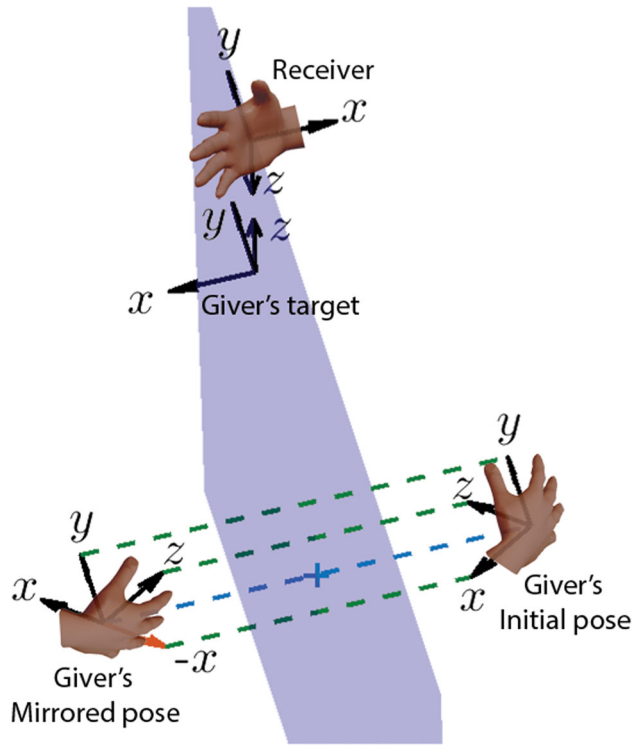


Fig. 2 Mirroring with respect to the target yz plane

less parameters, which leads to faster regression. During execution, appropriate mirroring actions are utilized each time the giver’s initial pose is associated with the side for which training was not performed.

Figure 1 displays both left and right hands with the hand frame adopted in this work; z – axis is perpendicular to the palm, with direction from the outer to the inner side of the palm, y – axis is perpendicular to the outer palm side denoted by the gray dashed line and finally x – axis is chosen so that the coordinate system is right-handed. Notice that, whether the hand is left or right, the hand’s orientation is the same. Thus, a recorded path in $SE(3)$ could come from either a right or a left hand. Given this convention for the hand orientation, we investigate the existence of mirroring about the yz target plane, shown in Fig. 2, by applying the reflection rules holding for the polar vectors and pseudovectors which are detailed in the following subsection. The giver’s target frame is derived from the receiver’s hand frame rotated by

180° around its y -axis, with a constant offset with respect to the receiver's hand frame biased towards the free object volume excluding the grasped part. Learning this offset is considered beyond the scope of this work.

3.1 Preliminaries on reflections for vectors and pseudovectors

Vectors or polar vectors have a specific transformational relation with the underlying basis of the space they are part of, whereas pseudovectors or axial vectors do not share this property. Polar vectors represent translational transformations whereas pseudovectors represent rotational transformations. In that sense a pseudovector's direction denotes the direction of rotation i.e. right-handed-ness versus left-handedness. Since a rotation co-relates the basis components of the space in a specific way unlike a translation (or scaling), pseudovectors change under a transformation in such a way as to maintain or compensate the representation they have i.e the direction (and magnitude) of rotation.

For some polar vector $r \in \mathfrak{R}^3$, the reflection about the subspace of all vectors orthogonal to $n \in \mathfrak{R}^3$ is performed as follows:

$$r_m = H(n)r \quad (12)$$

where $H(n)$ is the Householder matrix and the subscript m is utilized to denote the respective reflected vectors. For a unitary n , $H(n)$ is given by:

$$H(n) = I_3 - 2nn^T \quad (13)$$

with I_3 being the 3x3 identity matrix. In case of pseudovectors $s \in \mathfrak{R}^3$, reflection is performed as follows:

$$s_m = \det(H(n))H(n)s. \quad (14)$$

To reflect the giver's hand orientation expressed as a rotation matrix $R \in SO(3)$, given the axis convention utilized in this work, y and z axes of the giver's hand are reflected as polar vectors while the x axis as a pseudovector. Figure 2 demonstrates mirroring in the case of a right handed giver and receiver. It shows how the giver's hand frame in the initial pose is mirrored with respect to the yz target plane. As mirroring actions depend solely on the hand frame, the frames in Fig. 2 would remain the same if a left hand was used.

Moreover, the position and translational velocity are polar vectors whereas the angular velocity is a pseudovector. Polar vectors are reflected by applying (12), while pseudovectors are reflected by applying (14) (Fulling et al. 2011). In the case of mirroring with respect to the yz -plane $n = [1 \ 0 \ 0]$ and the reflection operator becomes $H(n) = \text{diag}[-1 \ 1 \ 1]$.

Thus, given the translational and angular velocities v , ω the mirrored velocities are given by:

$$v_m = [-v_x \ v_y \ v_z]^T \quad (15)$$

$$\omega_m = [\omega_x \ -\omega_y \ -\omega_z]^T. \quad (16)$$

3.2 Mirroring hypothesis validation

To test this hypothesis, we have selected 5 different initial giver poses and the respected mirrored poses and a fixed target (by fixing the receiver's pose). From each initial pose P we recorded 10 hand-over motions between humans to the fixed target, producing trajectories T_i , $i = 1 \dots 10$. We also recorded the corresponding hand-over motion from the mirrored pose P_m , producing trajectories T_{m_i} , $i = 1 \dots 10$. Using color markers at the demonstrator's hand the initial pose P was extracted using a kinect 1 sensor. The C++ library "VTK" was used to visualize this frame as well as the mirrored pose P_m that was computed analytically. Then, in each of the 10 repetitions, the demonstrator's hand placement was facilitated by ensuring that his hand's frame was visually close to that of P (or P_m for the motion starting from the mirrored pose). Nevertheless, this placement procedure yielded some initial errors in the pose's estimate. Moreover, the recorded trajectories differ slightly from one another due to the inherent variance in the human motions.

The recorded trajectories T_i were then aligned using Dynamic Time Warping (DTW) in order to have the same length (Amin and Mahmood 2008). For the DTW we used $d_n(p_1, p_2) + d_o(Q_1, Q_2)$ as distance metric between two poses p_1, Q_1 and p_2, Q_2 , where:

$$d_n(u, v) = \frac{1}{2} \frac{\|u - v\|^2}{\|u\|^2 + \|v\|^2} \quad (17)$$

is the normalized distance between vectors $u, v \in \mathfrak{R}^m$, and

$$d_o(Q_1, Q_2) = \text{norm}(e_o(Q_1, Q_2)) \quad (18)$$

with e_o given by (31). Then, we measured the distance between respective points in all trajectory pairs $\{T_i, T_j\}$ for $i \neq j$ yielding 45 distance trajectories; the Euclidean distance was utilized for positions and the cosine distance of the quaternions for the orientation. The mean plus/minus the standard deviation for each point of the distance trajectories was utilized to define a region expressing the admissible trajectory variability. Figure 3 illustrates the admissible region for two different initial poses (green regions). Notice that the admissible region becomes narrower as we get close to the target. This is attributed to inaccurate placement of the giver's hand in each initial pose P which yielded up to 7 cm initial errors for the position and $0.05 \in [0 \ 1]$

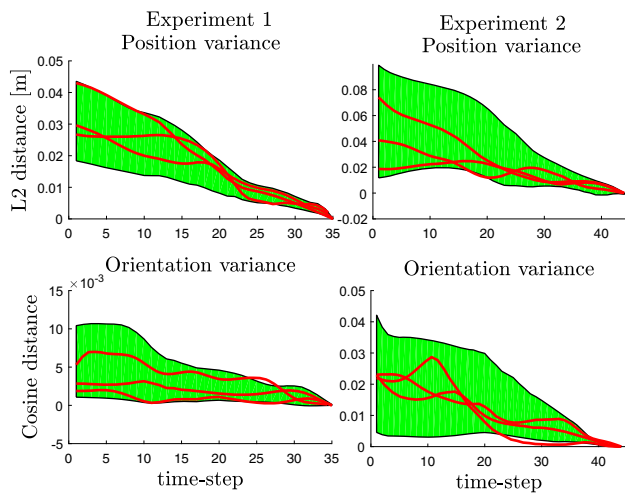


Fig. 3 Admissible region for two different initial poses (green regions) with examples of distance trajectories between $\{T_i, \hat{T}_{m_j}\}$ (red lines)

in the cosine distance and the fact that all trajectories converge to the same target as the motion evolves. Then, for each of the recorded T_{m_i} we have created by reflection \hat{T}_{m_i} and tested the mirroring hypothesis by checking whether the distance trajectories calculated from $\{T_i, \hat{T}_{m_j}\} \forall i, j$ belong to the admissible region. This procedure was repeated for the five different initial poses. Figure 3 shows with the red lines, examples of distance trajectories from $\{T_i, \hat{T}_{m_j}\}$. It can be observed that distance trajectories lie almost completely within the green region, which means that the error between a trajectory starting from P and its reflection starting from P_m has an error comparable to that of the variance attributed to measurement errors and the inherent variance in the human motion. Consequently, these experiments underpin our allegation of mirroring in human motions during hand-over.

Remark 2 Notice that mirroring would not be useful if there were demonstrations crossing significantly the yz -plane. However such handover scenarios are not expected since either an overly bended motion that would cross the yz -plane would be infeasible due to the arm's kinematic constraints and/or it would be highly unnatural for a human to perform such a curved motion without a reason, deviating from the target and then converging to it. In our demonstrations a marginal cross-over of the yz -plane was observed in the case a demonstration started very close to the yz -plane or when the hands of the giver and receiver came close to each other. As these cross-overs occur very close to the boundary of the yz -plane, their impact was found negligible.

3.3 Mirroring during execution

Let us assume that a DS is trained in the half space corresponding to $x < 0$. At the implementation stage, when mirroring actions are required we mirror the current pose

using (12), (14) as well as the model output using (15) and (16). Specifically, the pseudocode in Algorithm 1 describes the use of mirroring with the DS at the execution stage.

Algorithm 1: Pseudocode for mirroring in DS

Input : Current pose $p = [x \ y \ z]^T, R$
 Target pose $p_d = [x_d \ y_d \ z_d]^T, R_d$
 expressed in the same inertia frame, e.g. the camera frame.

Output: The desired velocity $V = [v^T \ \omega^T]^T$

- 1: Express all poses w.r.t. the target pose:
 Current pose: $\hat{p} = R_d^T(p - p_d) = [\hat{x} \ \hat{y} \ \hat{z}]$, $\hat{R} = R_d^T R$
 Target pose: $\hat{p}_d = [0 \ 0 \ 0]^T$, $\hat{R}_d = eye(3)$
- 2: **if** $\hat{x} > 0$
 mirrorOccured = **true**
 Mirror position using (12): $\hat{p} = [-\hat{x} \ \hat{y} \ \hat{z}]$
 Mirror orientation using (14) for the first column of \hat{R} and (12) for the last two columns:
 $\hat{R}(1, 2) = -\hat{R}(1, 2)$, $\hat{R}(1, 3) = -\hat{R}(1, 3)$
 $\hat{R}(2, 1) = -\hat{R}(2, 1)$, $\hat{R}(3, 1) = -\hat{R}(3, 1)$
 end
 mirrorOccured = **false**
 end
- 3: Calculate the quaternions \hat{Q}, \hat{Q}_d from the rotation matrices \hat{R}, \hat{R}_d
- 4: Calculate ξ , given by (3), using $\{\hat{p}, \hat{Q}\}, \{\hat{p}_d, \hat{Q}_d\}$
- 5: Calculate the velocity $V = [v^T \ \omega^T]^T$ from (4) given ξ
- 6: **if** **mirrorOccured** == **true**
 Mirror the output of the DS utilizing (15) and (16):
 $v = [-v_x \ v_y \ v_z]^T$
 $\omega = [\omega_x \ -\omega_y \ -\omega_z]^T$
 end

4 Dynamical system training and evaluation

4.1 Data acquisition

Fifty handover demonstrations were carried out. During these demonstrations an elderly person was chosen as the receiver and held his hand at a fixed pose waiting for an object to be handed over. An adult, holding an object, performed the reaching motion towards the receiver's hand, each time from a different initial pose. Our aim was to capture the relative hand pose of the giver with respect to the receiver and train a DS that outputs the desired linear and angular velocities given this relative hand pose. Our emphasis is on the direction of this learned velocity field rather than its magnitude, i.e. we are more concerned with the shape of the path that the DS produces given a relative hand pose rather than the movement's execution speed. The latter can be varied and adjusted by multiplying the DS output with a positive scaling factor without compromising the shape of the produced path or the systems's global asymptotic stability. We cov-

ered as many relative hand poses as possible in order to have a more complete dataset for training and testing and to be able to generalize well in the case of a moving target without the need of a predictor. The giver's hand motion was recorded by a kinect 1 sensor which tracked the position of 4 color markers that were attached on the giver's hand. Thus data for the 3D trajectory of the giver's reaching motion was captured. Out of the recorded demonstrations, 25 were taken from the subspace with $x < 0$ and used for the training of the DS and the rest were taken from different poses of the entire 3D space and used to test the accuracy of the learned model. For the training process, apart from position and orientation of the human wrist, the translational and angular velocities were obtained numerically. In fact, for two subsequent measurements $t_1, p(t_1), R(t_1)$ and $t_2, p(t_2), R(t_2)$, the translational velocity was calculated by $v(t_1) \approx \frac{p(t_2) - p(t_1)}{t_2 - t_1}$ and the angular velocity $\omega(t_1) \approx \frac{k \delta \theta}{t_2 - t_1}$, where $k, \delta \theta$ is the axis-angle representation of $R(t_2)R^{-1}(t_1)$. To alleviate the noise inserted due to the numerical differentiation, we then applied a moving average filter to the calculated velocities.

4.2 Performance metrics

The metrics employed to assess the accuracy of our trained model in comparison with the recorded demonstrations $\{\xi^{t,n}, V^{t,n}\}_{t=0, n=1}^{T_n, N}$, serve the purpose of quantifying how close the paths and velocity fields are from the learned model in comparison with the demonstrations. In fact, given the generalized position and velocity generated by the learned model P_1, V_1 and the generalized position and calculated velocity from the corresponding demonstration P_2, V_2 we define the following metrics:

$$M_1 = \frac{1}{T} \sum_{n=1}^N \sum_{t=0}^{T_n} d_1(P_1, P_2) \quad (19)$$

$$M_j = \frac{1}{T} \sum_{n=1}^N \sum_{t=0}^{T_n} d_j(V_1, V_2) \quad (20)$$

where $j \in \{2, 3\}$ is utilized to quantify the accuracy of the learned model in terms of both the direction and magnitude of the velocity, respectively. Given two vectors $u, v \in \mathfrak{N}^m$, we denote by $d_n(u, v) = \frac{1}{2} \frac{\|u-v\|^2}{\|u\|^2 + \|v\|^2}$ the normalized distance between u, v and by $d_c(u, v) = \left(1 - \frac{u^T v}{\|u\| \|v\|}\right)$ the cosine distance. Notice that $d_n(u, v), d_c(u, v) \in [0, 1]$. Hence, we define:

$$d_1(P_1, P_2) = \frac{1}{2} (d_n(p_1, p_2) + d_c(Q_1, Q_2))$$

$$d_2(V_1, V_2) = \frac{1}{2} (d_c(v_1, v_2) + d_c(\omega_1, \omega_2))$$

$$d_3(V_1, V_2) = \frac{1}{2} (d_n(v_1, v_2) + d_n(\omega_1, \omega_2))$$

Notice also that $M_1, M_2, M_3 \in [0, 1]$.

Before using any of these metrics, we first applied the DTW algorithm to align the trajectories to be compared.

4.3 Evaluation results

The aim of the evaluation is to show that a single dynamical system can be trained using only demonstrations from half the 3D space, while still being able to produce human-like and accurate motions in the entire 3D space via mirroring. The evaluation was performed by simulating kinematically a KUKA LWR4+ arm model in V-REP, following the scheme presented in Fig. 6. Specifically, for each initial pose of the demonstrations, we simulated the motion generated from our model and compared it against the human demonstrations. The aggregate results are presented in Table 1. All distance metrics exhibit small values close to zero, which implies that the trained model was able to reproduce efficiently the human motion both in the training and test data sets. The similar values of the distance metrics in the training and test sets indicate that the model is not overtrained. Representative examples from the train and test sets are shown in Fig. 4 where we plot the 3D paths generated by the human (dashed line) and the DS (solid line), enriched with frames expressing the orientation of the wrist. Notice that examples in the training set start from the trained region $x < 0$ whereas examples from the test set include both trained and unseen regions in which mirroring actions were performed. As we can observe, the trajectories produced by the DS almost coincide with that of the human.

To highlight the impact of using mirroring when the DS is trained in half the space, we further conducted two simulations from the untrained subspace ($x > 0$) and used the DS with and without incorporating the mirroring actions. Figure 5 shows the simulated paths together with the respective human demonstrations (blue lines); it does also include two cases from the trained subspace ($x < 0$) for comparison purposes. It is clear that without mirroring, the trajectories generated from the DS (dashed lines) fail to imitate the human motion although they converge to the target. By employing mirroring in these cases, the generated path is similar to that of the human.

Table 1 Evaluation results

Distance Metric	Training set	Test set
M_1	0.0177	0.0159
M_2	0.1708	0.199
M_3	0.1523	0.206

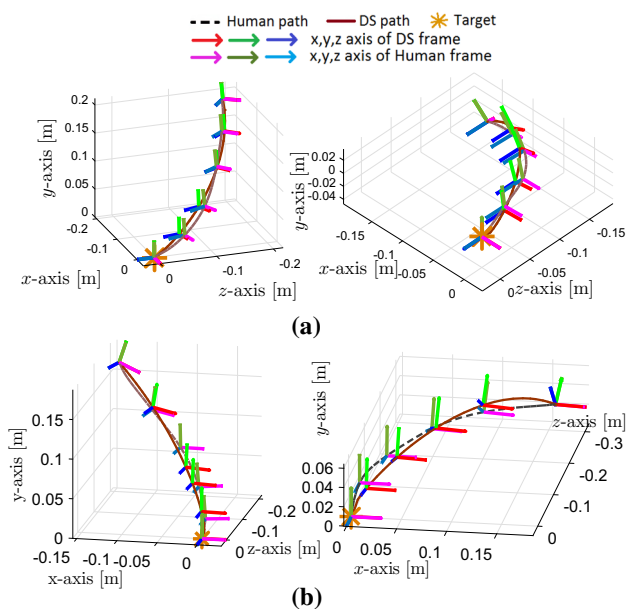


Fig. 4 Examples of DS generated paths from various initial poses to a fixed target pose and respective human paths from **a** the training set and **b** the test set. **a** Training set paths. **b** Test set paths

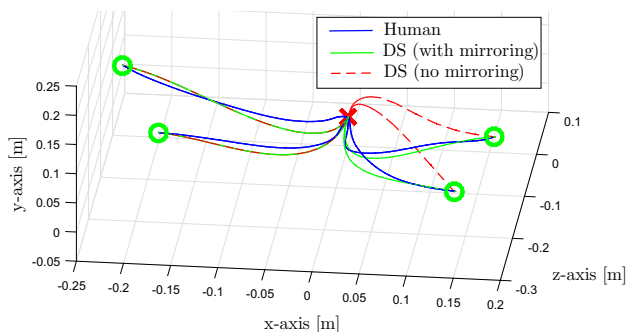


Fig. 5 Paths generated by the DS in trained and unseen regions with and without mirroring and respective human demonstrations (o : initial positions, x : target)

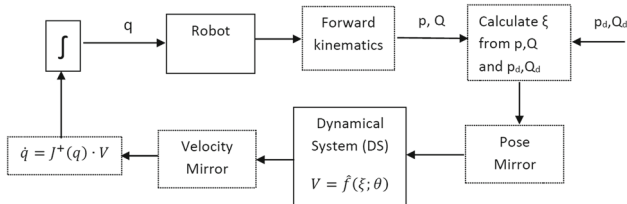


Fig. 6 Proposed control scheme

5 Object load transfer strategy

The object load transfer strategy proposed in Psomopoulou and Doulgeri (2015) considers the case of a robotic giver hand under a control law that achieves a stable grasp equilibrium state via fingertip rolling and accurate estimates of the object’s weight. A Lyapunov based theoretical analysis

performed for the overall system comprised by the object and the two hands of the giver and receiver shows that the system converges to a new attractive equilibrium. In the absence of a robotic hand with rolling fingertip capabilities, one can adapt the strategy of Psomopoulou and Doulgeri (2015) using force/torque sensing or estimation while keeping the basic concept that allows the safe object transfer. In particular and similarly to Psomopoulou and Doulgeri (2015) the strategy is receiver initiated in the sense that the giver follows closely the receiver’s lead in load transfer, ensuring haptically that the full load from the object’s weight has been transferred to the receiver. The initial state is that the robotic giver has already grasped an object and has an accurate estimation of the object’s weight via a force/torque sensor located on its wrist and that another hand (the receiver’s hand) is grasping the object. The strategy for the robot giver is to continuously estimate its load in the gravity direction and ensure the object’s load safe handover before releasing it. In this work, the latter is performed when the weight estimation crosses zero which means that the giver has been relieved from the object’s load. As during the approaching phase disturbance forces may arise that can jeopardize this haptic cue, visual sensing can be utilized to ensure that a joint grasp occurs. Notice that the proposed object load transfer strategy does not assume or require a stationary target as demonstrated in the experimental results.

6 Handover simulations

Handover simulations are carried out in V-REP using two KUKA LWR4+ robotic arms with a Barrett BH8 Hand attached to their wrists which are equipped with torque sensors at the finger’s last joints. The first one represents the robot (giver) and the second one is used to simulate the behavior of the human (receiver). During the handover, both participants move their arms according to the trained DS. Hence, we utilize the DS to also simulate the movement of the human-receiver. Although such a hypothesis about the receiver’s motion is not verified in our work, it is a human-like motion given that the DS was trained from human demonstrations and was able to replicate the human motion with sufficient accuracy. It is further assumed that the giver stably grasps an object during the approaching phase. Its target frame is associated with the receiver’s hand frame as perceived by the camera. When at target, the receiver closes the fingers with a predefined velocity until the reaction force sensed by the finger torque sensors exceeds a predefined threshold. Then, the receiver’s hand tries to move upwards taking the object load. The giver which is monitoring the object’s load at the gravity direction senses when the object load is fully transferred and releases its grip. After the handover completion, both arms retract.

Table 2 Giver's and receiver's target for each simulation case

Simulation case	Giver's target	Receiver's target
1: Moving target	Receiver's hand	Giver's hand
2: Mixed target	Receiver's hand	Final exchange site
3: Fixed target	Final exchange site	Final exchange site

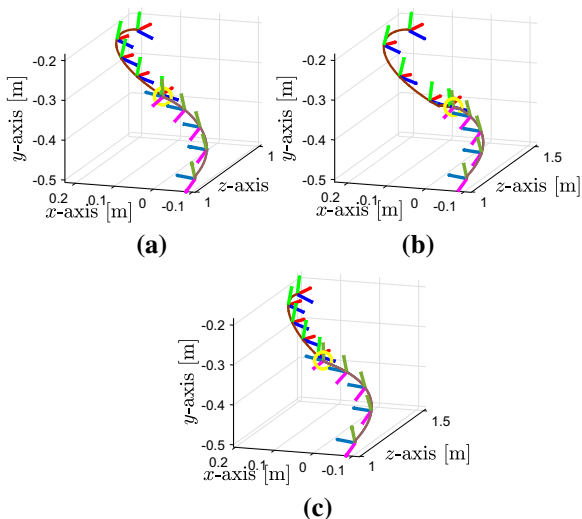
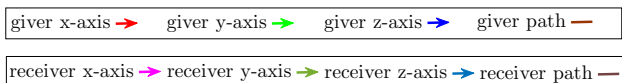


Fig. 7 3D oriented path of the human's and robot's hand during the approaching phase towards the target (yellow circle). **a** Case 1—moving target. **b** Case 2—mixed target. **c** Case 3—fixed target

To highlight our argument, that a natural handover can take place given that both participants share the collaborative intent to reach each other's hand, without any prior knowledge of the final exchange location, we carry out, at first, three handover simulation cases of a cylindrical object of mass 0.3 kg, height 22 cm and radius 4.4 cm. In all cases, the initial configurations of the giver's and receiver's arms was the same. Specifically, in the first case, both the giver and the receiver considered as target the current hand pose of each other; as a result the handover exchange takes place in an a priori unknown location. In the second case, the receiver regards as target an a priori known final exchange location, which was set at the exchange location resulting from the first simulation case. The assumption is that the receiver moves towards the predefined fixed exchange location irrespective of the giver's motion. Finally, in the third case both participants consider as target the fixed exchange location. These cases are summarized in Table 2.

The generated trajectories, paths, velocities and force responses are depicted in Figs. 7, 8, 9 and 10. The principal time instances of the first handover simulation are shown in Fig. 11. Examining the 3D paths of the giver and receiver

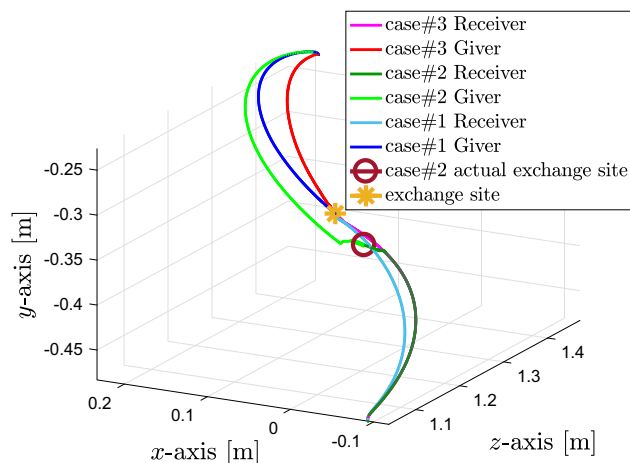


Fig. 8 3D paths of giver and receiver with respect to the camera frame during the approaching phase for each simulation case

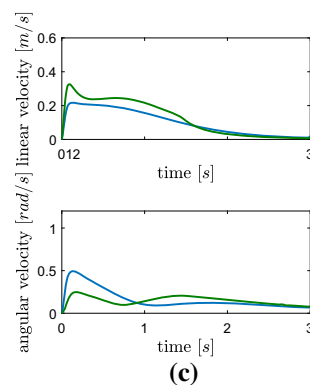
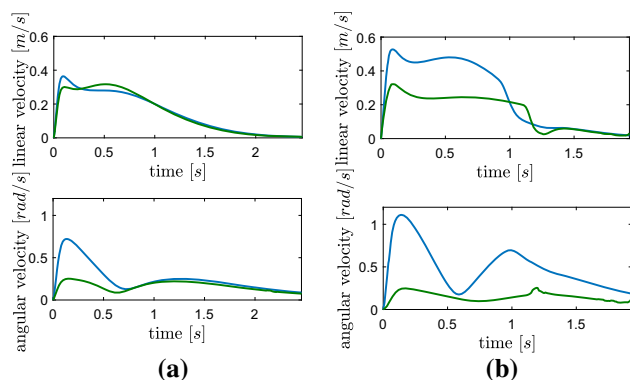


Fig. 9 Euclidean norm of linear and angular velocities of giver (blue line) and receiver (green line). **a** Case 1—moving target. **b** Case 2—mixed target. **c** Case 3—fixed target

during the approaching phase in Fig. 7 it is evident that the giver's path exhibits a wider bend in the second case Fig. 7b compared to the third case Fig. 7c where the final handover location was known a priori. This is exactly the undesired behavior pointed out in Widmann (2016) and (Prada and Remazeilles 2012) which encourages the prediction of the exchange site. However, the fact that the receiver was not

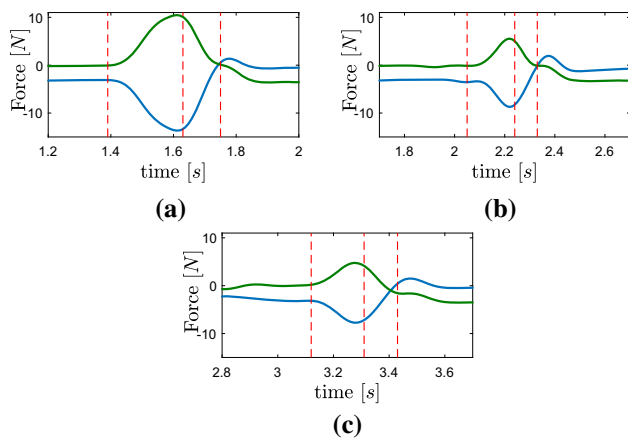


Fig. 10 Force sensed by the wrists of the giver (blue line) and the receiver (green line) in the gravity field during the object load transfer. **a** Case 1—moving target. **b** Case 2—mixed target. **c** Case 3—fixed target

very cooperative during the handover, in the sense that he doesn't take into consideration the giver's motion and just moves independently to a predefined location, accounts for the giver's excessive curved motion. Nevertheless the giver finally reaches the receiver's hand. Were the mutual consensus to reach the hand of the other participant also shared by the receiver, a more natural handover could be obtained. This is substantiated by the paths illustrated in Fig. 7a, where the presented paths resemble much more those from Fig. 7c. Still the giver's path in Fig. 7a appears slightly more curved than the path in Fig. 7c, but this should come as no surprise since the giver doesn't know beforehand where the receiver's hand will eventually stop. As the giver quickly adapts his motion thanks to the tacit consensus of both participants to move towards one another a natural handover takes place. All these remarks can be more easily discerned in Fig. 8, where we provide the 3D paths of giver and receiver for each simulation case, having omitted the orientation frames to avoid overcrowding the image. What is further revealed in Fig. 8 is that in the second case the exchange takes place at a location which differs from the predetermined receiver's target. This happens because the giver moves faster, as his target (receiver's hand) is further apart. As a result he reaches the receiver's hand, while the latter is in his way to his predetermined target. The lack of collaboration in reaching each other's hand (mainly from the receiver's part) produces less smooth responses as can be concluded from the paths in Fig. 8 and the velocities in Fig. 9. On the contrary, both the paths and the velocities of the giver and receiver appear quite smooth in the other cases.

Finally, Fig. 10 shows measurements of the wrist force-torque sensor from the giver and the receiver in the gravity direction. These measurements are estimates of the object's weight during the handover (the weight of the Barrett hand

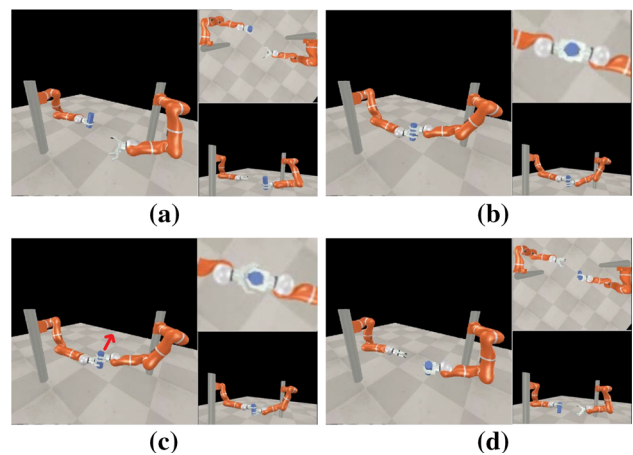


Fig. 11 Time instances from the 1st case handover simulation. In **c** the red arrow indicates the direction towards which the receiver pulls the object. **a** Giver grasps object. **b** Joint grasp. **c** Giver releases object. **d** Handover is complete

has been subtracted). We can distinguish two phases (denoted by the time span between the vertical dashed lines). The first denotes the time the receiver fingers close for grasping creating a disturbance load (in this case pushing slightly towards the gravity direction) before starting in the second phase to exchange the object load while pulling away. Figure 11(c) shows a snapshot of the V-REP at the joint object grasp and the direction of the receiver's hand pulling (red arrow). When the weight estimate crosses zero beyond a threshold value the giver releases the grip following the proposed strategy. Note that some vicissitudes observed during the object load transfer are because of the forces applied during contact that give rise to disturbances, while before and after the object load transfer are to be attributed to forces generated by the dynamics of the motion.

More simulations have been further performed for a moving target with different scenarios regarding the object geometry and weight, the motion velocity and consequently the reaching distances of the giver and the receiver as well as their relative initial poses. Figures 12–14 show respectively the 3D oriented path of the giver and the receiver, the euclidean norm of their linear and angular velocities during the approaching phase and the force sensed by their wrists in the gravity field during the object load transfer. The giver's velocity was scaled by 1.2 in all cases. Figures 12a, 13a and 14a correspond to a handover of a cuboid object of 0.1 kg with the receiver's velocity scaled by 0.7. Figures 12b, 13b, 14b depict a handover of a cylindrical object of 1 kg where the receiver is much slower (its velocity is scaled by 0.5). Notice the receiver's shortest path and the difference in the velocity magnitude in the respective figure plots.

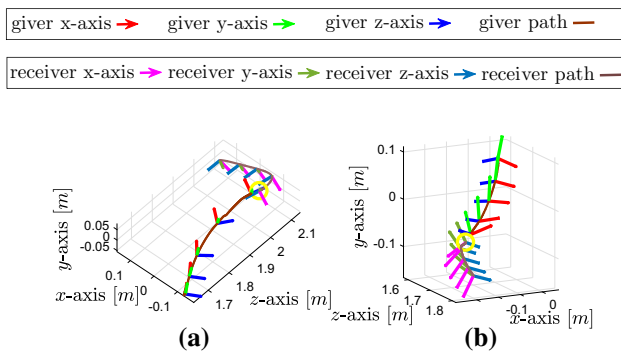


Fig. 12 3D oriented path of the human's and robot's hand during the approaching phase towards the target (yellow circle). **a** Lighter cuboid object. **b** Heavier cylindrical object

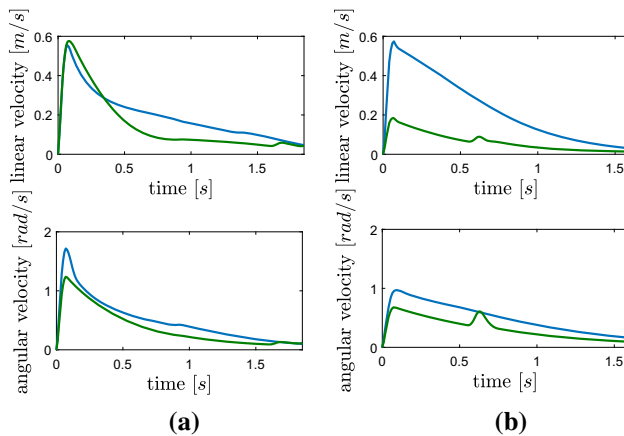


Fig. 13 Euclidean norm of linear and angular velocities of giver (blue line) and receiver (green line). **a** Lighter cuboid object. **b** Heavier cylindrical object

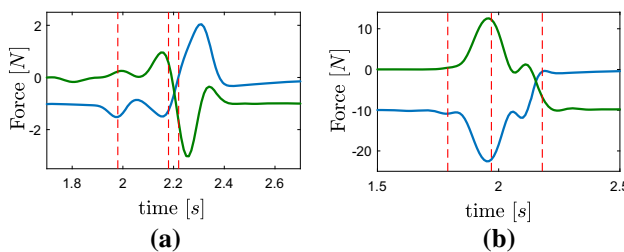


Fig. 14 Force sensed by the wrists of the giver (blue line) and the receiver (green line) in the gravity field during the object load transfer. **a** Lighter cuboid object. **b** Heavier cylindrical object

7 Handover experimental results

The proposed method was also evaluated in a real handover setting with a KUKA LWR4+ robotic arm, equipped with a Barret BH8 hand, handing over different objects to a left and right-handed human receiver. The robot motion is generated by the trained DS fed by the human's current hand pose as target with respect to the current robot's hand pose, which is calculated by the robot's forward kinematics. To track

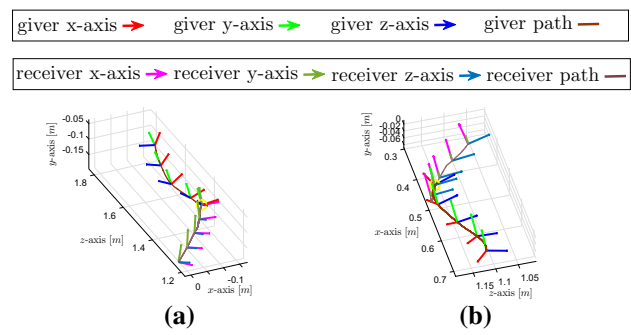


Fig. 15 Experimental results of the 3D oriented path of the human's and robot's hand during the approaching phase. The yellow circle denotes the final exchange site. **a** right-handed human receiving a bottle. **b** left-handed human receiving a box

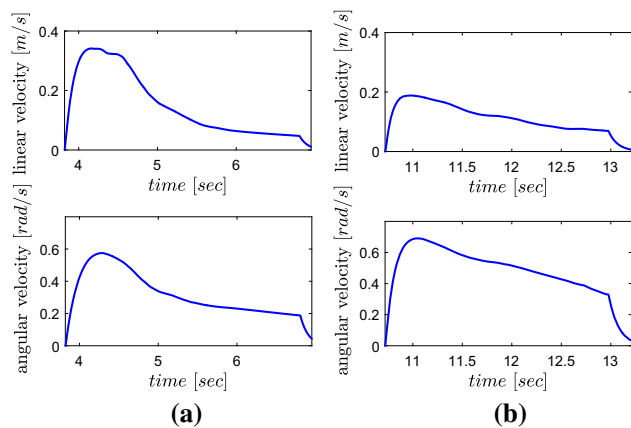


Fig. 16 Experimental results of the euclidean norm of linear and angular velocities of the robot giver. **a** Right-handed human receiving a bottle. **b** Left-handed human receiving a box

the human's hand pose, 4 AR tags attached at the human's hand are tracked by a stationary Kinect 1 sensor to increase the vision system's robustness. During the motion, KUKA's external force estimator is used to monitor the external force along the gravity direction. When this force crosses zero the hand opens its grip. We utilize the DS output to obtain the desired end-effector velocity V_d . In order to smooth the transition from the initially stationary robot to the initial desired velocity $V_d(0)$ which is generally not zero, velocity errors are passed from a first order filter utilizing a time constant that ensures fast convergence to the generated DS output $V_d(t)$. Then, we use the first order inverse kinematics to obtain the joint velocities which are integrated and given as joint references to KUKA. In case the object load transfer is completed with non zero velocities the robot is commanded to decelerate to zero and retract to the initial position.

Experimental results from two handover scenarios are presented in Figs. 15–17, where the 3D oriented paths of the human and the robot, the robot's velocity and its perceived force at the wrist are depicted. In the first experiment a right handed standing human receives a bottle of 0.3 kg, while, in

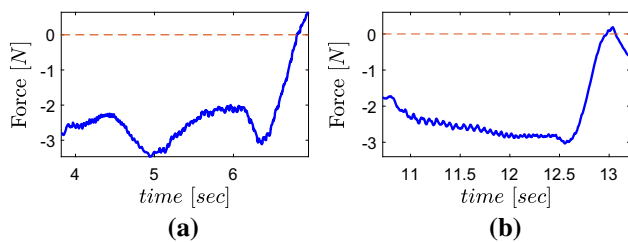


Fig. 17 Experimental results of the force sensed by the wrist of the robot giver in the gravity field during the object load transfer. **a** Right-handed human receiving a bottle. **b** Left-handed human receiving a box

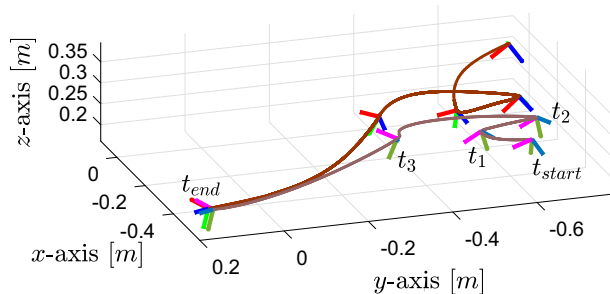
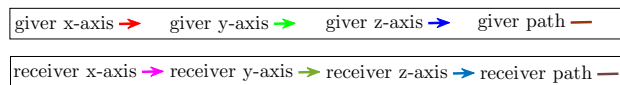


Fig. 18 Experimental results of the 3D oriented path of the human's and robot's hand during the approaching phase. The human changes his position and hand orientation at the time instances t_1 , t_2 , t_3 before receiving the object at time t_{end} .

the second experiment a left handed standing human receives a rectangular box of 0.25 kg. Figure 15 shows the 3D paths of the robot as well as the human path that is smoothed in order to alleviate the noise introduced by the vision system. In Fig. 16 we can see the robot's velocity which is gradually decreasing as it approaches the receiver's hand. Notice the fast deceleration to zero after the object load transfer is completed at $t = 3$ s in Fig. 16a and $t = 2.3$ s in Fig. 16b as indicated by the zero crossing of the force in Fig. 17. Last, a complex hand-over case is performed with a user purposely changing his hand position and orientation three times after the robot has initiated his approaching motion as shown in Figs. 18–20. Despite the unrealistic scenario, the advantages of the proposed method are clearly demonstrated. The human changes his hand pose at time instances t_1 , t_2 , t_3 shown in Fig. 18 before receiving the object at time t_{end} . In Fig. 19 the corresponding linear and angular velocity of the robot is depicted, where we can see the velocity norm decreasing as the robot approaches the human's hand and increases again when the human moves away. Finally, in Fig. 20 the instant the handover takes place is indicated by the zero crossing of the sensed force in the gravity direction. These experiments

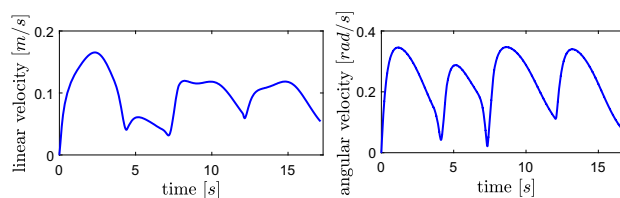


Fig. 19 Experimental results of the euclidean norm of linear and angular velocities of the robot giver

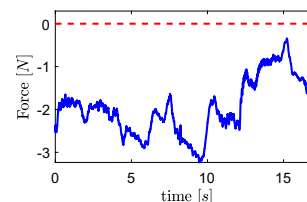


Fig. 20 Experimental results of the force sensed by the wrist of the robot giver in the gravity field during the object load transfer

together with other scenarios are included in the uploaded video.

8 Conclusions

In this work, an approach for stable robot to human handover is presented utilizing a dynamical system and an object load transfer strategy that ensures full load transfer before grip release. The dynamical system encodes human wrist position and orientation during handovers from a set of demonstrations to a fixed target. DS training takes advantage of the mirroring revealed by our study. Evaluation results show that human motion is reproduced efficiently based on three performance metrics regarding positions and velocities. It is shown that the proposed DS can execute successfully and naturally handovers even in the case of a moving receiver, without the need to predict the final exchange site. We validate our method by conducting handover simulations in V-REP using two KUKA LWR4+ robotic arms with a Barrett Hand model attached to their wrists to model the giver and receiver. We have also demonstrated the efficacy of the proposed approach experimentally utilizing a KUKA LWR4+, different objects and left and right handed human receivers. As a future work we aspire to apply the proposed DS to bi-manual manipulations.

Appendix: Unit quaternion preliminaries

A four-parameter representation of the orientation is the unit quaternion defined as $Q = [\eta \epsilon^T]^T$ with $\eta \in \mathfrak{R}$ being the scalar part and $\epsilon \in \mathfrak{R}^3$ the vector part and which are related with the angle-axis representation of orientation,

$r \in \mathfrak{R}^3$, $\theta \in \mathfrak{R}$ as follows:

$$\eta = \cos \frac{\theta}{2} \quad (21)$$

$$\epsilon = r \sin \frac{\theta}{2} \quad (22)$$

Notice that utilizing the angle-axis representation, one specific rotation can be expressed with two different ways: a rotation by $-\theta$ around $-r$ or a rotation by θ around r . On the contrary, utilizing the quaternion representation there is a unique expression for each rotation (Siciliano et al. 2010). The following properties hold for unit quaternions:

$$Q^T Q = 1 \quad (23)$$

$$Q^T \dot{Q} = 0 \quad (24)$$

$$Q^{-1} = \begin{bmatrix} \eta \\ -\epsilon \end{bmatrix} \quad (25)$$

Composition of unit quaternions $Q_1 = [\eta_1 \ \epsilon_1^T]^T$ and $Q_2 = [\eta_2 \ \epsilon_2^T]^T$, denoted by the operator $*$, yields the unit quaternion corresponding to the respective rotation matrix product $R_1 R_2$ where $R_1, R_2 \in SO(3)$:

$$Q_1 * Q_2 = \begin{bmatrix} \eta_1 \eta_2 - \epsilon_1^T \epsilon_2 \\ \eta_1 \epsilon_2 + \eta_2 \epsilon_1 + \epsilon_1 \times \epsilon_2 \end{bmatrix} \quad (26)$$

Given the current and desired rotation matrices $R \in SO(3)$, $R_d \in SO(3)$ as well as the respective quaternions Q, Q_d , the relative rotation RR_d^T , can be defined in terms of the quaternion $\Delta Q = [\Delta \eta \ \Delta \epsilon^T]^T$ as follows:

$$\Delta Q = Q * Q_d^{-1} \quad (27)$$

Notice that $\Delta Q = [1 \ 0_{1 \times 3}]^T$ if and only if $R_d = R$.

Unit quaternion time derivatives are related to the angular velocity ω expressed in the inertia frame as follows (equations (3.94)-(3.95) from Siciliano et al. (2010)):

$$\begin{aligned} \dot{\eta} &= -\frac{1}{2} \epsilon^T \omega \\ \dot{\epsilon} &= \frac{1}{2} (\eta I_3 - \hat{\epsilon}) \omega \end{aligned} \quad (28)$$

which can be written compactly as:

$$\dot{Q} = \frac{1}{2} J_Q \omega \quad (29)$$

where

$$J_Q = \begin{bmatrix} -\epsilon^T \\ \eta I_3 - \hat{\epsilon} \end{bmatrix} \in \mathfrak{R}^{4 \times 3}. \quad (30)$$

Given (26)–(27), a minimal representation of the orientation error $e_o \in \mathfrak{R}^3$ can be defined via the vector part of the quaternion error as follows:

$$e_o \triangleq \Delta \epsilon = \eta_d \epsilon - \eta \epsilon_d - \hat{\epsilon} \epsilon_d \quad (31)$$

with $\hat{\epsilon}$ denoting the skew symmetric matrix of vector ϵ . Notice that (31) can be written as:

$$e_o = -J_Q^T Q_d \quad (32)$$

Substituting (29) in (24) yields $J_Q^T Q = 0$; thus, e_o can be written also in the following form:

$$e_o = J_Q^T (Q - Q_d). \quad (33)$$

References

- Amin, T.B., & Mahmood, I. (2008). Speech recognition using dynamic time warping. In *2nd International conference on advances in space technologies* (pp. 74–79).
- Arimoto, S. (2008). *Control theory of multi-fingered hands: A modelling and analytical-mechanics approach for dexterity and intelligence*. London: Springer.
- Ben Amor, H., Neumann, G., Kamthe, S., Kroemer, O., & Peters, J. (2014). Interaction primitives for human-robot cooperation tasks. In *IEEE International Conference on Robotics and Automation (ICRA)* (pp. 2831–2837). IEEE (Online). Available <http://ieeexplore.ieee.org/document/6907265/>.
- Bischoff, R., & Guhl, T. (2010). The strategic research agenda for robotics in Europe [industrial activities]. *IEEE Robotics Automation Magazine*, 17(1), 15–16.
- Cakmak, M., Srinivasa, S. S., Lee, M. K., Forlizzi, J., & Kiesler, S. (2011). Human preferences for robot-human hand-over configurations. In *IEEE/RSJ International Conference on Intelligent Robots and Systems* (pp 1986–1993).
- Calinon, S., D'halluin, F., Sauser, E. L., Caldwell, D. G., & Billard, A. G. (2010). Learning and reproduction of gestures by imitation. *IEEE Robotics Automation Magazine*, 17(2), 44–54.
- Chan, W. P., Parker, C. A., Van der Loos, H. M., & Croft, E. A. (2012). Grip forces and load forces in handovers. In *Proceedings of the seventh annual ACM/IEEE international conference on Human-Robot Interaction: HRI '12* (pp. 9–16).
- Chan, W. P., Parker, C. A., Van der Loos, H. M., & Croft, E. a. (2013). A human-inspired object handover controller. *The International Journal of Robotics Research*, 32(8), 971–983.
- Fulling, S. A., Sinyakov, M. N., & Tishchenko, S. V. (2011). *Linearity and the mathematics of several variables*. Singapore: World Scientific.
- Gribovskaya, E., & Billard, A. (2009). Learning nonlinear multi-variate motion dynamics for real-time position and orientation control of robotic manipulators. In *9th IEEE-RAS International Conference on Humanoid Robots* (pp. 472–477).
- Gribovskaya, E., Khansari-Zadeh, S., & Billard, A. (2011). Learning non-linear multivariate dynamics of motion in robotic manipulators. *The International Journal of Robotics Research*, 30(1), 80–117.
- Hersch, M., Guenter, F., Calinon, S., & Billard, A. (2008). Dynamical system modulation for robot learning via kinesthetic demonstrations. *IEEE Transactions on Robotics*, 24(6), 1463–1467.

- Huber, M., Rickert, M., Knoll, A., Brandt, T., & Glasauer, S. (2008). Human–robot interaction in handing-over tasks. In *RO-MAN 2008: The 17th IEEE International Symposium on Robot and Human Interactive Communication* (pp. 107–112). IEEE.
- Ijspeert, A. J., Nakanishi, J., & Schaal, S. (2002). Movement imitation with nonlinear dynamical systems in humanoid robots. *Proceedings 2002 IEEE International Conference on Robotics and Automation (Cat. No.02CH37292)*, 2, 1398–1403.
- Khansari Zadeh, S. M., & Billard, A. (2009). *Learning and control of uav maneuvers based on demonstrations*. Presented at Robotics Science and Systems, Seattle, June 28 July 1, 2009.
- Khansari-Zadeh, S. M., & Billard, A. (2010). Imitation learning of globally stable non-linear point-to-point robot motions using nonlinear programming. In *2010 IEEE/RSJ International Conference on Intelligent Robots and Systems (IROS)* (pp. 2676–2683).
- Kim, I., Nakazawa, N., & Inooka, H. (2002). Control of a robot hand emulating human's hand-over motion. *Mechatronics*, 12(1), 55–69.
- Kupcsik, A., Hsu, D., & Lee, W. S. (2015). Learning dynamic robot-to-human object handover from human feedback. In *International Symposium on Robotics Research* (pp. 1–11) (Online). Available <http://arxiv.org/abs/1603.06390>.
- Lang, M., Kleinstueber, M., Dunkley, O., & Hirche, S. (2015). Gaussian process dynamical models over dual quaternions. In *European Control Conference (ECC)* (pp. 2847–2852).
- Mason, A. H., & MacKenzie, C. L. (2005). Grip forces when passing an object to a partner. *Experimental Brain Research*, 163(2), 173–187.
- Medina, J. R., Duvallet, F., Karnam, M., & Billard, A. (2016). A human-inspired controller for fluid human-robot handovers. In *Conference: 2016 IEEE-RAS International Conference on Humanoid Robots*.
- Murray, R., & Sastry, S. (1994). *A mathematical introduction to robotic manipulation*. Boca Raton: CRC Press.
- Pastor, P., Hoffmann, H., Asfour, T., & Schaal, S. (2009). Learning and generalization of motor skills by learning from demonstration. In *IEEE International Conference on Robotics and Automation* (pp. 763–768).
- Pastor, P., Kalakrishnan, M., Meier, F., Stulp, F., Buchli, J., Theodorou, E., & Schaal, S. (2012). From dynamic movement primitives to associative skill memories. *Robotics and Autonomous Systems*.
- Pastor, P., Righetti, L., Kalakrishnan, M., & Schaal, S. (2011). Online movement adaptation based on previous sensor experiences. In *IEEE/RSJ International Conference on Intelligent Robots and Systems* (pp. 365–371).
- Prada, M., & Remazeilles, A. (2012). Dynamic movement primitives for human robot interaction. In *IEEE/RSJ IROS, workshop on robot motion planning: online, reactive and in Real-time, Algarve, Portugal*.
- Prada, M., Remazeilles, A., Koene, A., & Endo, S. (2013). Dynamic movement primitives for human-robot interaction: Comparison with human behavioral observation. In *IEEE/RSJ international conference on intelligent robots and systems* (pp. 1168–1175).
- Prada, M., Remazeilles, A., Koene, A., & Endo, S. (2014). Implementation and experimental validation of dynamic movement primitives for object handover. In *IEEE/RSJ International Conference on Intelligent Robots and Systems* (pp. 2146–2153).
- Psomopoulou, E., & Doulgeri, Z. (2014). A robot hand-over control scheme for human-like haptic interaction. In *22nd Mediterranean conference of control and automation (MED)* (pp. 1470–1475).
- Psomopoulou, E., & Doulgeri, Z. (2015). A human inspired stable object load transfer for robots in hand-over tasks. In *IEEE/RSJ international conference on intelligent robots and systems (IROS)* (pp. 491–496).
- Shukla, A., & Billard, A. (2012). Coupled dynamical system based armhand grasping model for learning fast adaptation strategies. *Robotics and Autonomous Systems*, 60(3), 424 – 440. Autonomous Grasping (Online). Available <http://www.sciencedirect.com/science/article/pii/S0921889011001576>.
- Siciliano, B., Sciacovo, L., Villani, L., & Oriolo, J. (2010). *Robotics: modeling, planning and control*. London: Springer-Verlag Limited.
- Silverio, J., Rozo, L., Calinon, S., & Caldwell, D. G. (2015). Learning bimanual end-effector poses from demonstrations using task-parameterized dynamical systems. In *IEEE/RSJ International Conference on Intelligent Robots and Systems (IROS)* (Vol. 2015, pp. 464–470). IEEE.
- Sisbot, E. A., Marin-Urias, L. F., Broquère, X., Sidobre, D., & Alami, R. (2010). Synthesizing robot motions adapted to human presence. *International Journal of Social Robotics*, 2(3), 329–343. <https://doi.org/10.1007/s12369-010-0059-6>.
- Strabala, K., Lee, M. K., Dragan, A., Forlizzi, J., Srinivasa, S., Cakmak, M., et al. (2013). Towards seamless human-robot handovers. *Journal of Human-Robot Interaction*, 1(1), 1–23.
- Ude, A., Nemeč, B., Petri, T., & Morimoto, J. (2014). Orientation in Cartesian space dynamic movement primitives. In *IEEE International conference on robotics and automation (ICRA)* (pp. 2997–3004).
- Waldhart, J., Gharbi, M., & Alami, R. (2015). Planning handovers involving humans and robots in constrained environment. In *IEEE/RSJ international conference on intelligent robots and systems (IROS)* (pp. 6473–6478).
- Wang, R., Wu, Y., Chan, W. L., & Tee, K. P. (2016). Dynamic movement primitives plus: For enhanced reproduction quality and efficient trajectory modification using truncated kernels and local biases. In *IEEE/RSJ International conference on intelligent robots and systems (IROS)* (pp. 3765–3771).
- Widmann, D. (2016). *An adaptive control approach based on dynamic movement primitives for human-robot handover*. Masters thesis in Systems, Control and Mechatronics, Chalmers University of Technology, Department of Signals and Systems, Gothenburg, Sweden.



Antonis Sidiropoulos received his diploma in 2016 from the Electrical and Computer Engineering (ECE) Department of Aristotle University of Thessaloniki (AUTH), Greece and he is currently a PhD student in the same department. In 2017 he worked as a researcher at the research institute CERTH-ITI. His research interests include nonlinear dynamical systems and robust adaptive control, machine learning and analysis and design of algorithms.



Efi Psomopoulou graduated from the Department of Electrical and Computer Engineering at Aristotle University of Thessaloniki in 2010 and received her PhD from the same department in 2017. In the period 2015–2017 she worked as a researcher at the research institute CERTH-ITI and she is currently a research associate in Bristol Robotics Laboratory, UK. Her research has been focused on object grasping and manipulation by robot fingers as well as on human-robot object hand-over.

She is also working on the control of flexible joint robots with variable elasticity and the non-model based control of robotic systems with prescribed performance guarantees.



Zoe Doulgeri received her diploma from the Electrical and Computer Engineering (ECE) department of Aristotle University of Thessaloniki (AUTH), Greece and her MSc in Control Systems and her PhD in production scheduling of flexible manufacturing systems from the Imperial College, London UK. She is currently a Professor in Robotics and Control of Manufacturing Systems in the Electrical and Computer Engineering Dept. of AUTH and a collaborative professor with the

research institute CERTH-ITI. She is the author of more than 100 scientific papers in international journals and refereed conference proceedings. She served as Associate editor at the *Journal of Intelligent and Robotic Systems* (2012-2015) and she is currently an Associate editor in the *Frontiers in Robotics and AI* and the *IEEE Robotics and Automation Letters*. Her research interests include physical human-robot interaction, object grasping and manipulation, redundant and flexible joint manipulators, and model free control of robotic systems with prescribed performance guarantees. She is an IEEE Senior member (RAS and CS), the representative of Greece in the European Control Association (EUCA) and a member of the Technical Chamber of Greece.